

A SINGLE LAYER SILICON-ON-INSULATOR MEMS GYROSCOPE FOR WIDE DYNAMIC RANGE AND HARSH ENVIRONMENT APPLICATIONS

Michael Kranz^{*a}, Tracy Hudson^{**b}, Paul Ashley^b, Paul Ruffin^b, Sherrie Burgett^b,
Mark Temmen^c, Jerry Tuck^c

^aMorgan Research Corp., Huntsville, AL; ^bU.S. Army Aviation and Missile Command, Huntsville, AL; ^cThe Aegis Technologies Group, Huntsville, AL

ABSTRACT

The Army Aviation and Missile Command (AMCOM), Morgan Research Corporation, and Aegis Research Corporation are developing an SOI-based vibratory-rate z-axis MEMS gyroscope utilizing force-feedback control, and intended for wide dynamic range and harsh environment applications. Rate sensing in small diameter ballistic missile guidance units requires a rate resolution of less than 1°/hr over a range of -3000 to +3000°/sec, resulting in a dynamic range of 10⁷. In addition, the devices must operate through military specifications on temperature (-55°C to +125°C) and vibration (1000g at 5-15kHz). This paper presents modeling, simulation, and fabrication efforts, as well as initial test data, for an SOI-based rate sensor intended for this application. The prototyped gyroscope is a single layer structure consisting of a proof mass placed in a three-fold mode-decoupled symmetric suspension. The device is fabricated in a cost-effective and highly-controllable Silicon-on-Insulator (SOI) process for in-plane inertial devices. The mechanical structure is integrated in a vacuum-sealed hermetic package with a separate CMOS readout ASIC. At the present time, the device has undergone two design iterations, with the most recent just completed.

Keywords: MEMS, Vibratory-Rate Gyroscope, Silicon-On-Insulator, Sigma-Delta Modulator

1. Introduction

Many organizations are exploring MEMS-based gyroscopes for rate sensing applications, with numerous devices being demonstrated and reported in the literature. To a large extent, these efforts have been focused on achieving certain levels of bias stability, resolution, and/or random walk using surface micromachining techniques^{1,2,3,4}, or bulk/hybrid micromachining techniques^{5,6}. However, there are existing applications that require wide dynamic range operation, as well as operation through large temperature swings and vibrational environments.

In particular, the newest generation of Army missile systems will see ever increasing extremes in operational and environmental conditions. The missile system on which the MEMS device described in this paper will be installed has some particularly extreme requirements. The missile system is a guided munition that experiences a large roll-rate about its longitudinal axis during flight. The anticipated rotational rates encompass a range of -3000°/sec to +3000°/sec. In order to control the heading of this system during guided flight, the system must know its roll angle about the longitudinal axis so that control systems can adjust accordingly. The accuracy of this angular measurement must correspond to a bias stability of 1°/hr in order for the guidance systems to compensate.

Furthermore, the actuators in the control system of the missile result in a substantial vibration environment. Large shocks of greater than 4000g can be seen at frequencies in the 1kHz to 15 kHz range. Various attenuation and mounting techniques are being proposed to reduce that requirement to greater than 800g's in that frequency range. In either event, that shock environment can play havoc on a MEMS roll rate sensor, given that the sensor must operate accurately throughout those ranges.

* MKranz@morganres.com; phone 1 256 533 3233; Morgan Research Corporation, 4811A Bradford Dr, Huntsville, AL, USA 35805;

** Tracy.Hudson@ws.redstone.army.mil; ph 1 256 876-6242; AMCOM, AMSAM-RD-WS-ID, Redstone Arsenal, AL, USA 35898.

The Army is exploring many potential solutions to this control problem. Special vibration attenuating packaging, active vibration cancellation at the device level, and shock compensation at a signal processing level are all being explored. This paper will discuss a fourth technique under investigation, the device-level development of robust MEMS roll-rate sensors that are not susceptible to these shocks and vibrations, yet still able to meet the accuracy and dynamic range requirements.

The prototyped gyroscope presented in this paper is a single layer structure consisting of a proof mass placed in a three-fold mode-decoupled symmetric suspension with matched fundamental oscillation modes. When excited in one mode, rotations about the z-axis result in oscillations in the orthogonal mode. The mode-decoupled suspension allows only one degree of in-plane freedom for each excitation actuator, thereby attenuating errors due to oscillation axis misalignment. In addition, suspension symmetry maintains matched oscillation mode frequencies through processing and temperature variations, allowing maximized dynamic range in a wide dynamic range discrete-time control loop. Attached to the suspension are comb-drives operating in their linear mode. Use of these actuators eliminates deflection-induced nonlinearity in the control loop.

The device is fabricated in a cost-effective and highly-controllable process for in-plane inertial sensors. The process begins with a silicon-on-insulator wafer having a 100µm thick silicon layer on top of a 1µm thick oxide. This, in turn, sits on a standard silicon handle wafer. A thick photoresist mask is patterned on the wafer using standard lithography. Deep Si RIE is performed to define the microstructure. After the deep etch and removal of photoresist, the device undergoes a sublimation-based release process with a post-release anti-stiction coat that reduces process-induced and in-use stiction. After release, metallization is evaporated onto the surface to create electrical contacts. The mechanical structure is integrated in a vacuum-sealed hermetic package with a separate CMOS readout ASIC.

2.Theoretical Background

As seen in much of the literature relating to MEMS rotational rate sensors, and repeated here for completeness, the sensing method used in a vibratory-rate gyroscope is based on the Coriolis pseudo-force resulting from a translating body in a rotating frame of reference.

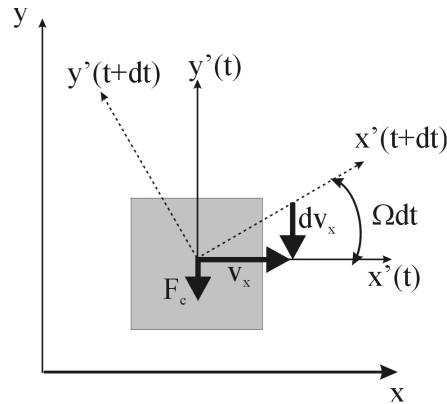


Figure 1 – Vibratory-Rate Gyroscope Rate Sensing Principle

As seen in Figure 1, a mass, m , is moving at time, t , with a velocity, v_x , along both the (x,y) and (x',y') axes. At time $t+dt$, the (x',y') axes have rotated an angle of Ωdt , where Ω is the rotational rate. In accordance with Newton's Laws, the mass is still moving with velocity, v_x , in the (x,y) frame of reference. However, in the (x',y') frame of reference, it appears that the velocity, v_x , has moved by an amount of dv_x . Therefore, the Coriolis acceleration and force is:

$$a_c = \frac{dv_x}{dt} = -2\Omega v_x \quad (1)$$

$$F_c = ma_c = -2m\Omega v_x \quad (2)$$

The fundamental result from this simple derivation of the dynamics of the system is that a translating mass in a rotational frame of reference will appear to, within the rotating frame, experience a force orthogonal to its velocity and proportional to its velocity and the rate of rotation of that frame of reference. A MEMS vibratory-rate gyroscope, as well as other vibration-based inertial sensors such as Hemispherical Resonator Gyroscopes (HRG's) uses this result to develop a signal proportional to rotational rate.

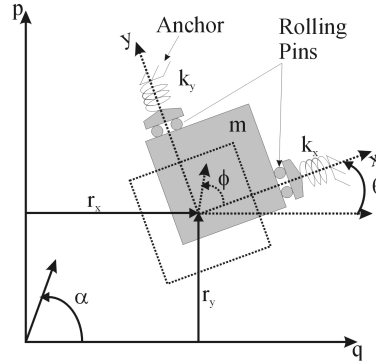


Figure 2 - Variable Definitions and Gyroscope Principle

A simplified version of a typical vibratory-rate gyroscope and its associated set of variables are shown in Figure 2. The device consists of a mass-spring system that has at least two orthogonal modes of oscillation. The mass, m , is forced to have a sinusoidal velocity in the frame of reference of the device, along the x -axis, for example. Springs k_x and k_y provide a suspension that constrains the mass to particular orthogonal oscillation modes. When the device experiences a rotation, the Coriolis force induces oscillation of the mass orthogonal to its original velocity. Sensors detect this motion and provide a signal from which the rotational rate is extracted.

The equations of motion for a mass-spring system moving in a non-inertial reference frame are found using Lagrangian dynamics⁷. First, expressions for the potential energy and kinetic energy of the system must be found. The variables used in the expressions are shown in Figure 2. The global frame of reference is the p - q - α frame, the local frame of reference, x - y - ϕ , is rotated by an angle, θ , with respect to the global frame. The local frame is also translated by r_x and r_y with respect to the global frame.

The potential energy stored in the springs is:

$$PE = \frac{1}{2} k_x x^2 + \frac{1}{2} k_y y^2 + \frac{1}{2} k_\phi \phi^2 \quad (3)$$

The kinetic energy is calculated in the global frame of reference, using the global variables:

$$KE = \frac{1}{2} m \left(\frac{dq}{dt} \right)^2 = \frac{1}{2} m \left(\frac{dp}{dt} \right)^2 + \frac{1}{2} I \left(\frac{d\alpha}{dt} \right)^2 \quad (4)$$

The global variables are related to variables in the local frame of reference by rotation matrices:

$$q(t) = \cos(\theta)x(t) - \sin(\theta)y(t) + r_x(t) \quad (5)$$

$$p(t) = \sin(\theta)x(t) + \cos(\theta)y(t) + r_y(t) \quad (6)$$

$$\alpha(t) = \theta(t) + \phi(t) \quad (7)$$

The equations of motion (EOM's), in the local frame of reference, are found from:

$$F_{x_i} = \frac{\partial L}{\partial x_i} - \frac{d}{dt} \frac{\partial L}{\partial \dot{x}_i} \quad (8)$$

where x_i are the generalized coordinates, F_{x_i} are external forces such as the damping and excitation forces, and L is the Lagrangian ($L=KE-PE$).

The global coordinates in the kinetic energy relation are substituted by (5), (6), and (7) to convert to local coordinates. Equation (8) is then applied for each of the on-chip coordinates, (x , y , ϕ), by replacing the generalized coordinate by the respective on-chip coordinate, yielding:

$$\ddot{y} = -\omega_y^2 y - \frac{\omega_y}{Q} \dot{y} - 2\Omega \dot{x} + y\Omega^2 - x\dot{\Omega} + a_x \sin \theta - a_y \cos \theta \quad (9)$$

$$\ddot{x} = -\omega_x^2 x - \frac{\omega_x}{Q} \dot{x} - \frac{F_x}{m} + x\Omega^2 + y\dot{\Omega} + 2\Omega \dot{y} - a_x \cos \theta - a_y \sin \theta \quad (10)$$

$$I\ddot{\phi} = -k_\phi \phi - I\ddot{\theta} \quad (11)$$

where $\omega_x^2=k_x/m$, and $\omega_y^2=k_y/m$, are the resonant frequencies of the x and y modes, respectively, a_x and a_y are external accelerations, and Q is the quality factor of resonance. The Coriolis accelerations reside in the $2\Omega y$ and $2\Omega x$ terms. The last two terms in (9) and (10) are acceleration terms, which create transients at the natural frequency of the system. The terms $y\dot{\Omega}$ and $x\dot{\Omega}$ refer to the inertia of angular acceleration. The $y\Omega^2$ and $x\Omega^2$ are centripetal accelerations, and act as spring softeners.

The importance of this derivation is that it includes extra terms in the EOM's above and beyond the standard Coriolis force terms. Under the large rotational rates and angular accelerations experienced in the application, these extra terms, the centripetal acceleration, linear acceleration, and angular accelerations, play larger roles in the error of the rotational rate signal. In addition, the derivation shows, as is commonly known, the role of matching resonant frequencies so that the benefits of a high quality factor can be applied to the sensor.

3. Mechanical Sensing Element

The rate sensor's mechanical sensing element is shown in Figure 3. In the design, a central proof mass is surrounded by a three-fold symmetric suspension consisting of identical spring sets along both the x and y modes. The comb-finger actuators apply an electrostatic force to the proof mass in the x -direction, exciting the driven mode. When experiencing an external rotational rate, the Coriolis force acts along y and has a frequency equal to that of the excitation frequency. The Q -factor of the system provides a gain in the displacement of the sensed mode. The y deflection is sensed with a pair of comb-finger capacitors connected as a differential capacitive voltage divider. A transimpedance amplifier (TZA) detects the currents in the capacitive divider and drive off-chip electronics.

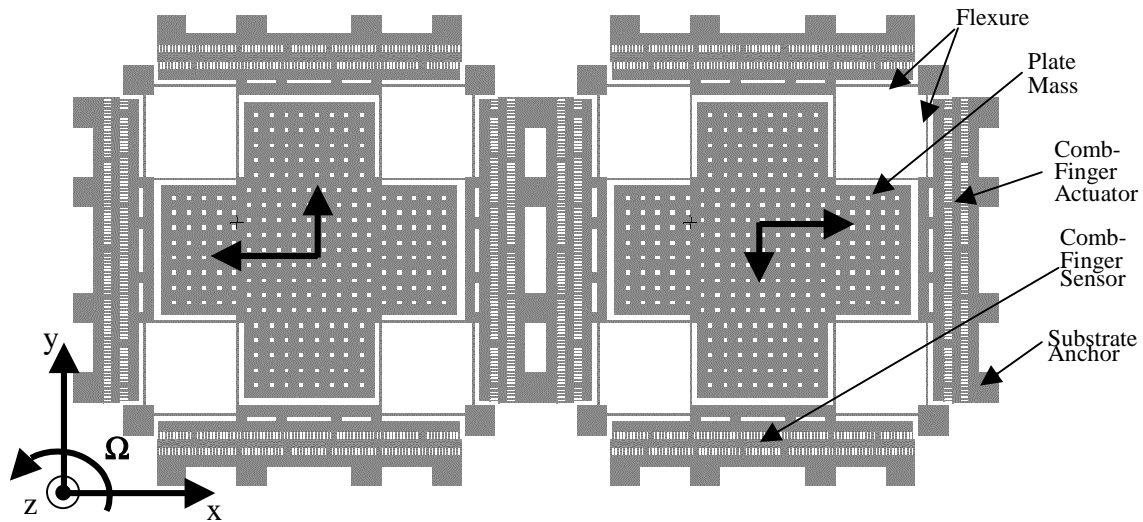


Figure 3 - Layout of Mechanical Sensing Element

The suspension is three-fold symmetric in that there is symmetry along y , along x , and along the device diagonal. The suspension serves two purposes. First, the driven and sensed modes of the device displace different, but identical, spring sets; one set displaces in x and one set displaces in y (See Figure 4, a finite-element simulation of the oscillation modes of the first design). Spring constants as well as moving mass are matched along both the excitation and sense modes. Therefore, both oscillation modes have equal resonant frequencies. The modes will theoretically match even through a uniform process variation, *e.g.*, over-etching of the proof mass, and through time and temperature variations.

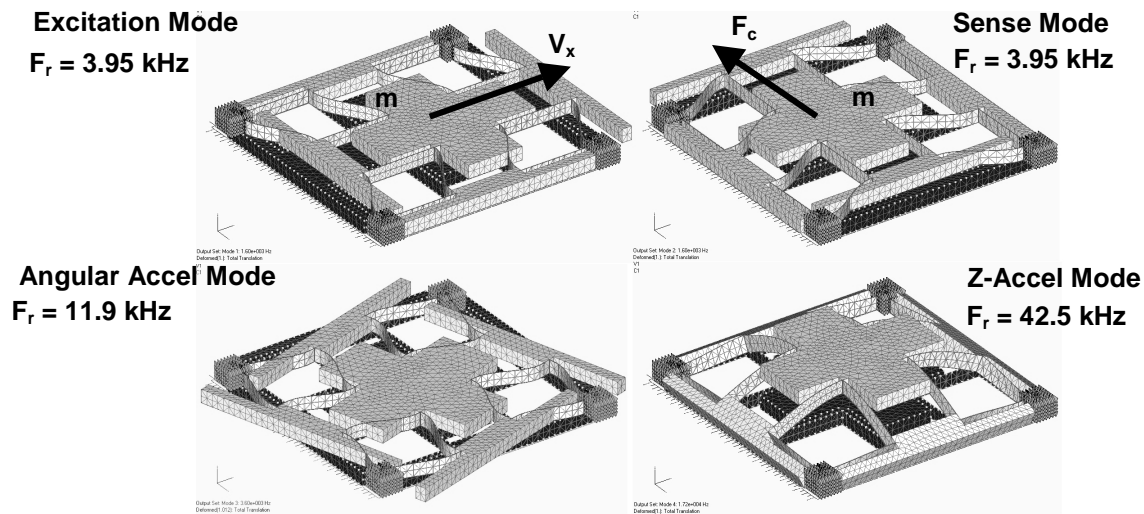


Figure 4 - Finite Element Analysis of the first four fundamental oscillation modes

The second purpose of the suspension is to de-couple, mechanically, the x and y deflections of the actuators and sensors. The suspension allows motion of the central mass in both x and y by using complete springs that are very stiff in one direction and very compliant in the other, as an approximation to a rolling pin. The masses that attach to the actuators and sensors are placed in the suspension in such a way that they can only move along one axis. So, a deflection of the proof mass in x will not affect the sense mass, which only moves in y . Therefore, the spring network reduces the mechanical cross-talk between the sensors and actuators. There is second-order cross-talk, however. When the proof mass displaces in x , the sense masses pull in towards the proof mass because of the constant length of the connecting beams (see Figure 5).

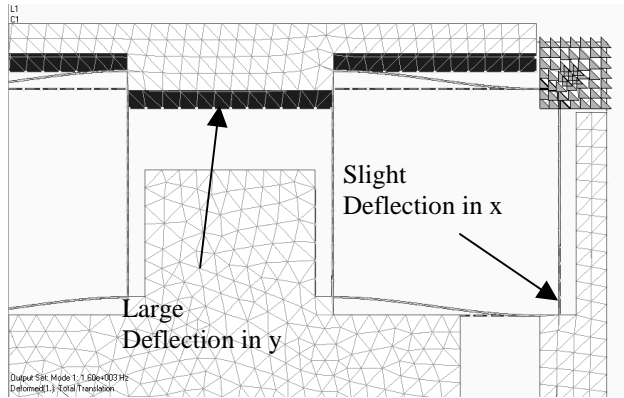


Figure 5 - View of second-order mechanical crosstalk

The three-fold symmetric gyroscope implementation inherently matches the resonant frequencies in both oscillation modes by using a completely symmetric suspension, thereby increasing the sensitivity of the device by using the Q -factor to maximize displacements for a given force. The symmetry also reduces effects of process variations on the device sensitivity. In practical implementations of the vibratory-rate gyroscope, the designed Q value is constrained by the necessary bandwidth of the input rotation. The scale factor of the device is highly dependent on the matching of the resonant frequencies, since Q is an important gain. If the frequencies are not matched, only a fraction of Q will be seen as gain. Through time and temperature variations, changes in the modes of this device should match, preventing the scale factor from drifting. Manufacturing variations and offsets may cause some mismatch of the modes, however, so electrostatic tuning may be implemented to compensate.

4. Fabrication Process

The fabrication process flow is shown in cross-section in Figure 6. The process begins with a simple SOI wafer. The wafer consists of a 100 micron tall device layer on a 1 or 2 micron thick oxide layer. These layers sit on a normal silicon handle wafer. A single mask is developed from the device layout and used to expose a layer of photoresist spun on top of the SOI's device layer. A deep silicon (Si) reactive ion etch (RIE) transfers the photoresist pattern to the device layer. After deep etching, a standard HF etch releases the structure from the substrate. A unique sublimation process is performed to avoid stiction due to liquid surface tensions. Due to the large amount of device surface area, an anti-stiction coating of HMDS is applied to discourage stiction occurring during device operation.

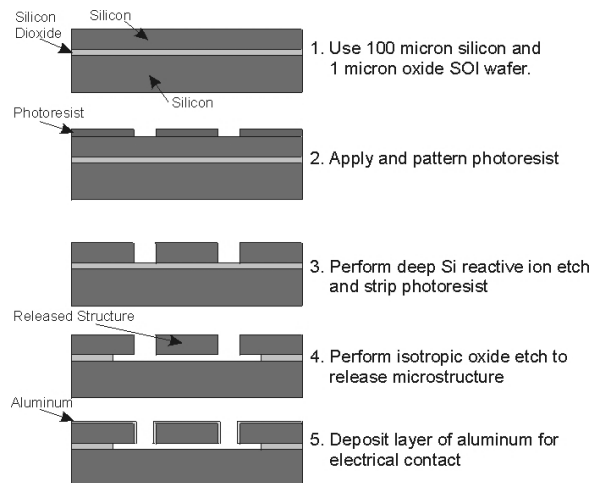


Figure 6 - Current SOI process flow

The SOI fabrication has a number of advantages for inertial sensor work. The process creates very thick and stiff structures out-of-the-plane of the chip. The advantage is in the robustness of the device to external shocks and vibrations. The current device moves only fractions of a micron during 1000g out-of-plane accelerations. In addition, out-of-plane vibrations are attenuated and resonances are far above the fundamental oscillation modes. The large thickness also yields large inertial masses that reduce noise sources due to Brownian motion. Large capacitive surface areas can also be developed due to the high aspect ratio of the deep Si etch. Finally, the process is inexpensive in that only one mask is required.

Using a deep trench structure in the 100 micron thick active layer, the sidewall angle was measured to be between 0.57 degrees and 1.00 degrees. This was determined by measuring the width of the bottom of the trench and the width at the top of the trench. The value is consistent with standard reports from the etching equipment used for this particular deep etch. With this particular sidewall angle, one would expect nearly a 100:1 aspect ratio. This is because the etch was able to go 100 microns down while only cutting inward 1 micron. However, this aspect ratio does not hold under narrow trench conditions because of limitations on etchant flow in those trenches. In reality, using characterization structures with varying width trenches, the maximum aspect ratio that resulted in well-etched and releasable structures was 25:1.

The first sets of devices released were extremely large in surface area. As a result, strong surface tension forces in the liquids used in the release process created release stiction. To avoid stiction, a number of design changes were made. First, the device was fabricated in a 100 micron thick active layer rather than 50 micron. This increased the structure's out-of-plane stiffness, as well as allowed the structure to have the required mass with less surface area, further reducing the stiction force and increasing resistance to it.

Secondly, two unique sublimation processes were used. In the first process, the final rinse fluid is frozen using a LN2 cooled platen onto the chip prior to evaporation. The solid is then placed in a vacuum chamber, pumped down, and sublimated. This process is therefore able to skip the surface tension that causes stiction. The second process is very similar other than having a different operating temperature. The second process used tertiary butanol to perform the final device rinse after release. Tert butanol is a solid at room temperature. It had to be heated prior to rinsing, but then cooled at near ambient temperatures. This greatly reduces materials' costs in the release process. After the tert butanol solidified, the solid structure was placed in a vacuum HMDS oven, which pumped down so the tert butanol could sublimate. Then, without breaking vacuum, the device was coated with HMDS to prevent in use stiction.

5. Multi-Bit Sigma-Delta Force Feedback Control

If operating in an open-loop mode, this sensor can demonstrate excellent noise performance, but will possess a large dynamic range. In open-loop mode, the readout electronics can potentially resolve angstroms of motion. This would represent a signal level at the minimum detectable rotational rate. If experiencing 10^7 times the minimum rate, which is the dynamic range required in the device, the mechanical sensing element would be displacing with an amplitude of 1 mm. This is clearly not achievable on this small of a device. However, if placed within a force feedback loop, where a force is developed that cancels the input force, the dynamic range can be extended.

This particular design utilizes a sigma-delta control loop architecture. Sigma-delta control has been demonstrated previously on accelerometers with a low resonant frequency^{8,9}. Sigma-delta control operates by applying a constant amplitude pulse width modulation signal at a frequency much above the resonant frequency of the sensing element. As the input force to the system increases, the width of the force pulses increase to cancel out that input force. Therefore, the dynamic range of a traditional sigma-delta controller is set by the ratio of minimum force pulse width, as determined by the maximum frequency of the control loop, and the maximum force pulse width, as determined by the resonant frequency of the system.

For many accelerometers, this control architecture can deliver a large dynamic range. This is because the sensing element in an accelerometer can be designed with a low resonant frequency, sometimes as low as 5 Hz. If the control

operates at a high frequency, a large pulse width ratio can be developed. However, for a vibratory-rate gyroscope, the larger the resonant frequency, the larger the signal-to-noise ratio. Therefore, it is beneficial to operate these devices at resonances of upwards of 4 kHz, almost three orders of magnitude higher. This resonance range also makes the device less susceptible to the military vibration environment. However, large resonant frequencies severely cut into the dynamic range of a sigma-delta controller.

To increase the dynamic range, it is possible to provide not only pulse width control on the force pulse stream, but to also provide pulse height control. In this scenario, as the input Coriolis force increases, the pulse widths can increase first. If the pulse width increase is not sufficient to cancel the input force, the pulse heights can begin increasing. The combination of increasing pulse width and amplitude can dramatically improve dynamic range. In this case, the dynamic range is set by the minimum pulse width amplitude possible, and the maximum pulse width and amplitude possible. For example, if the amplitude of the pulse train can be controlled with 12-bit accuracy, there are roughly amplitudes available to the control system, yielding 4000 times the dynamic range.

Figure 7 shows a block diagram of the control system being developed for this rotational rate sensor. The gyroscope is designed such that a high-frequency carrier signal can be input across the capacitive position sensors. This carrier is then picked up and multiplied by G_2 , the transimpedance amplifier. The signal is demodulated and filtered and provided as an input to the multi-bit A/D. This A/D sends a digital signal to the DSP, which then applies digital compensation for control loop stability. After compensation is applied, a digital signal is sent to the correct D/A to apply the appropriate force pulse to the appropriate electrostatic actuator. The output of the system is a signal from the DSP, and consists of a low-frequency digital bitstream representing decimated A/D data.

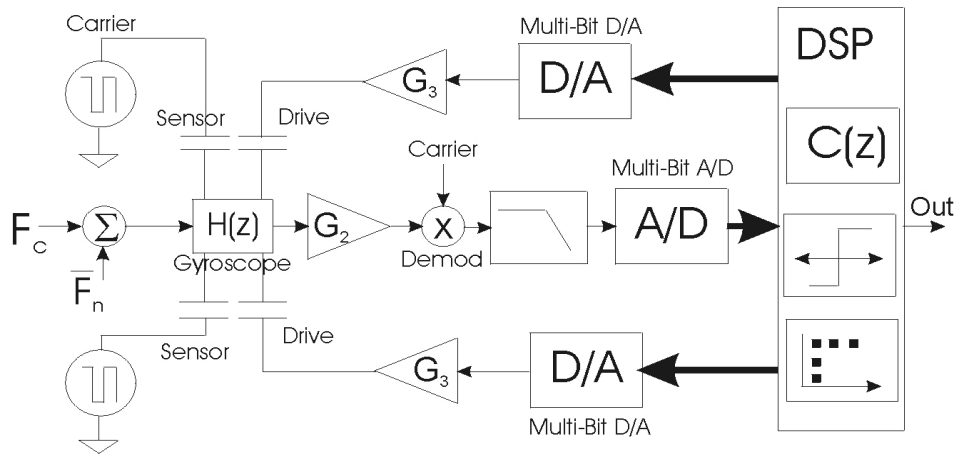


Figure 7 – Block Diagram for Multi-Bit Sigma-Delta Control Loop

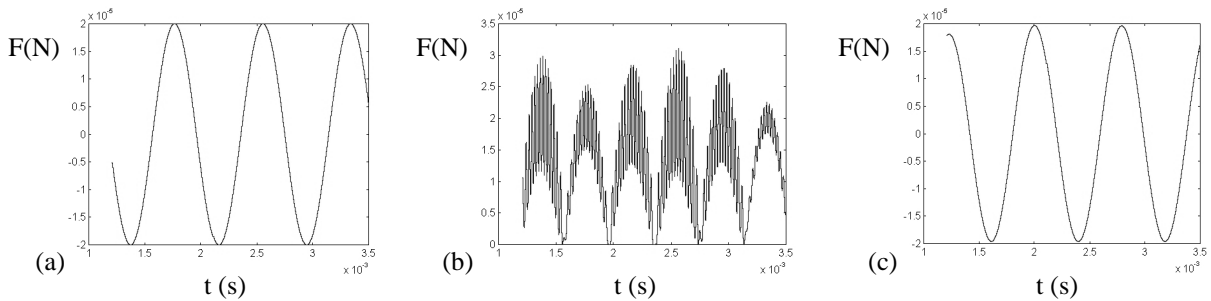


Figure 8 – System Simulation Under Maximum Rotational Rate

Figures 8(a,b,c) show simulations of the system experiencing a large rotational rate on the order of $2000^\circ/\text{sec}$. Figure 8(a) shows the Coriolis force due to the rotation. Figure 8(b) is the output of the D/A that drives the actuator. In this plot, both the force pulse amplitude and pulse width are changing. Figure 8(c) shows the resulting output signal after decimation and digital filtering.

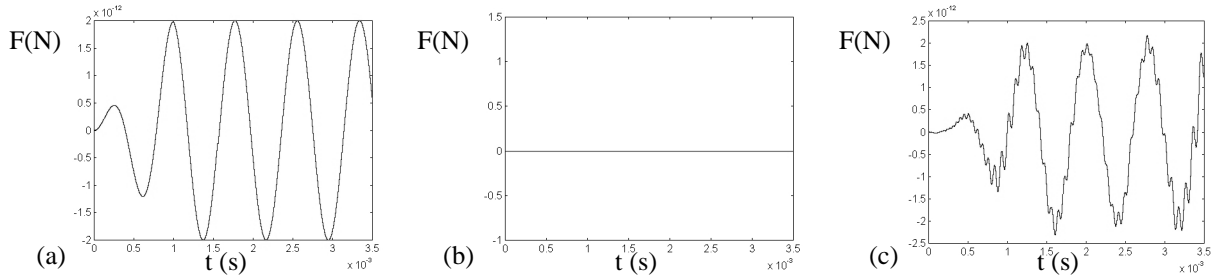


Figure 9 - System Simulation Under Minimum Rotational Rate

Figures 9(a,b,c) show simulations on the other end of the operational range. These plots are for rotational rates on the order of $0.1^\circ/\text{hr}$. Again Figure 9(a) is the input Coriolis force. Figure 9(b) shows the amplitude of the force pulses. In the low end of the signal range, the pulse amplitudes remain constant and the system operates like a simple one-bit sigma-delta controller. Figure 9(c) shows the output signal after decimation and filtering. The actual device noise can now be seen on this signal.

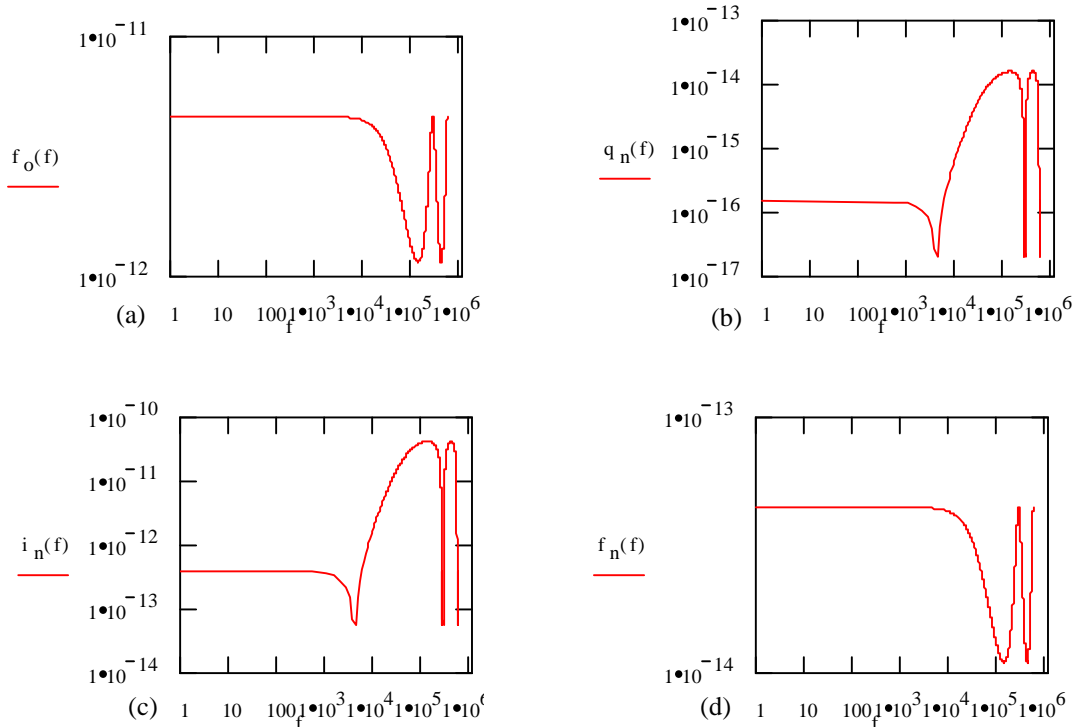


Figure 10 – Contributions to the System Output Due to Various Signal and Noise Sources

This control system has other benefits besides wide dynamic range. Furthermore, its design has been optimized for performance with the mechanical sensing element. Figure 10 shows, in a graphical sense, the contributions of various signals and noise sources to the overall system output. Figure 10(a) shows the contribution of the input Coriolis force. This is the signal of interest, and in this particular plot, is set at the minimum signal level that must be resolved. Figure 10(b) shows the contribution of quantization noise to the system output. The use of the multi-bit system has greatly

reduced quantization noise as compared to a single-bit implementation. In this case, quantization noise is negligible when compared to the input signal level. Figure 10(c) shows the contribution of amplifier current noise to the overall signal. The sigma-delta controller greatly attenuates this noise source in the frequency range of interest, which is a distinct advantage. Finally Figure 10(d) shows the contribution of Brownian motion to the overall signal. In this system, there is no attenuation of Brownian noise. Therefore, the mechanical structure must be designed and packaged in such a way as to minimize this noise source and push it below the amplifier current noise.

A major drawback of multi-bit sigma-delta modulators lies in the nonlinearity of the D/A converters used. In the one-bit versions of the system, the D/A is inherently linear since there are only two possible states, 0 and 1. In the multi-bit case, however, there are many possible states of the D/A, and these states may not be linearly related. The nonlinearities in the D/A's in this system are then seen as nonlinearities in the scale factor. This is a potential problem due to the strict requirements placed on scale factor linearity for these devices in military applications. To compensate for D/A nonlinearity, this system employs digital error correction. Prior to gyroscope operation, the D/A's are cycled through all possible levels. The A/D then reads the actual voltages at all of these levels. The digital representations of these voltages are then placed in a high-speed RAM. During gyroscope operation, these calibrated voltage levels are used in place of the voltage levels measured during operation.

6.Results and Device Characterization

At the writing of this paper, the rate sensor mechanical element has been fabricated, readout electronics have been designed and built, and the feedback control system designed, simulated, and prototyped. Figure 11 shows SEM's and photos of the mechanical sensing element and various features of the structure. Figure 11(a) is an SEM of a complete sensing element, which makes up one half of the entire MEMS portion of the gyroscope. Figure 11(b) shows a close-up of the deep Si RIE. Figure 11(c) shows a sensing element in a package and integrated with a PCB version of the readout electronics for characterization on a probestation.

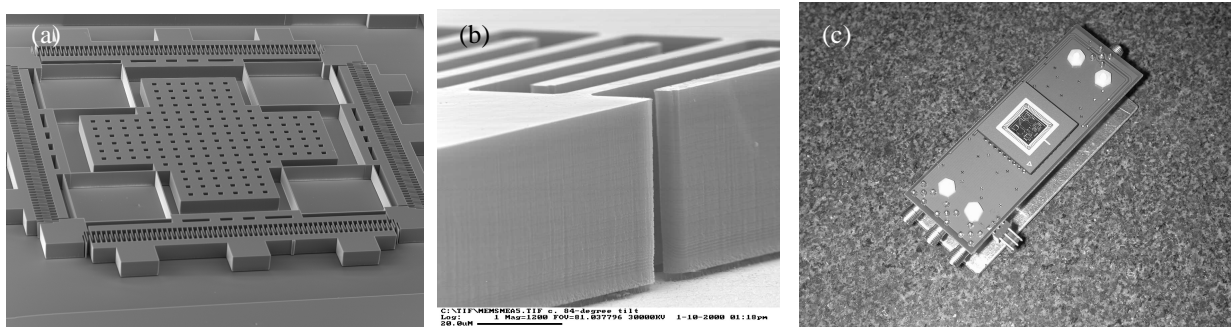


Figure 11 – Fabricated and Packaged Structures and Devices

The devices shown in these figures were characterized on a probestation to determine various performance specifications. Resonant frequencies of 4.550 kHz were measured. These are slightly above the 3.95 kHz expected. Most of this difference is due to nonlinear behavior of the structure. In order to increase the signal-to-noise ratio, this device is designed to operate with an excitation amplitude of nearly 100 microns. However, the fixed-fixed beams used in this suspension became nonlinear at around 10 microns.

Figure 12 shows data taken with the device under the probestation at atmospheric pressure. The resonance peak is easily seen at 4.5 kHz. The linear increase in the plot is due to the effects of parasitic capacitance, feedthrough, and pickup. All of these have a linear dependence on frequency and add to the output signal. Figure 13 shows a plot of resonance when the device was pumped down to a pressure of 25 mtorr. The width of the peak has greatly decreased from the test at atmospheric pressure. This is due to the removal of the dissipative gas surrounding the structure. This plot was used to determine a value for the expected quality factor of the device. At 1 atm, the Q was measured at 35, but at 25mtorr, Q

was measured to be 1500. This value of Q is lower than expected and is due to operation of the device in its nonlinear region.

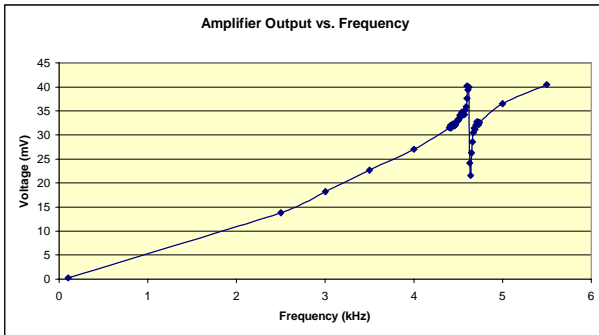


Figure 12 – Frequency Sweep at 1atm

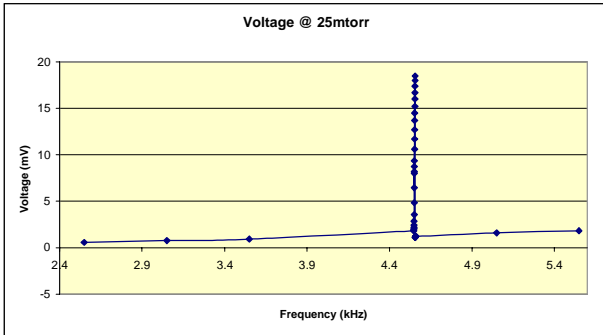


Figure 13 – Frequency Sweep at 25mtorr

When operated under normal operating conditions, the structure exhibited characteristics similar to that of a nonlinear resonator. This was evident in the resonance curve, which exhibited a large amount of hysteresis. Figure 14 shows a close-up of the resonance curve during a sweep of increasing then decreasing frequency. The resonance is easily seen. However, the sudden drop in amplitude just after resonance during an increasing sweep of frequency is more typical of a nonlinear resonator. In addition, under a decreasing frequency sweep, a jump to resonance occurred at a different frequency. For this device, performing these tests yielded a hysteresis curve with a sudden increase in amplitude at 4.552 kHz, rather than at 4.556kHz.

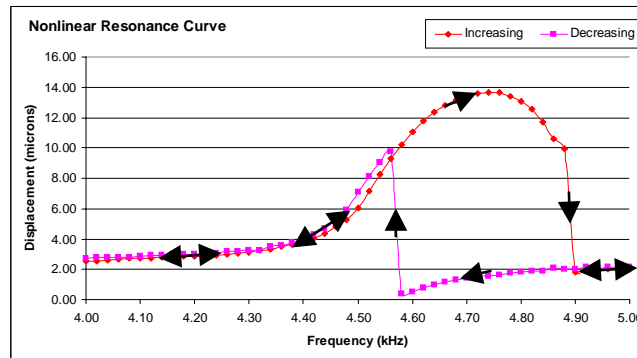


Figure 14 – Nonlinear Oscillator Behavior

7.Future Work

In order to complete this sensor development, a number of tasks must be completed and are listed below:

- The sensing element must be packaged in a hermetic package and vacuum-sealed
- The entire system must be integrated and run through functional tests
- The integrated device must undergo rigorous environmental tests
- The system must be optimized for performance and robustness
- All control and readout electronics should be implemented in an ASIC form

After completion of the sensor development, which is scheduled to be within the next two years, the device must then be fully characterized using Army test equipment and procedures. The device can then be integrated into advanced Army missile systems.

8. Summary and Conclusions

This paper presents an effort to improve, at the device level, the performance of MEMS vibratory-rate gyroscopes with respect to military requirements, and especially those of the newest generation of advanced Army missiles. The effort is exploring innovative design of the mechanical structure and the control electronics to widen the system's dynamic range and reduce its susceptibility to large external shocks and vibrations.

To date in this effort, it has been shown that various aspects of the mechanical structure, including symmetry, mode-decoupling, linear control actuators, and increased mechanical sensitivity, can lead to performance enhancements. In addition, a multi-bit sigma-delta control system with digital error correction has been proposed, simulated, and prototyped to extend the sensors dynamic range to levels required for high roll-rate missile systems. Finally, new and optimized SOI-based fabrication techniques have improved the mechanical structure and sensing system with respect to its performance requirements.

The device under development in this effort is based on a silicon-on-insulator mechanical sensing element. This sensing element has been fabricated and characterized both at atmospheric pressure and under a vacuum. Various parameters, including resonant frequency, quality factor, and parasitic values have been measured and calculated. In addition, a set of readout electronics has been designed and implemented on a PCB as well as in ASIC form. Finally, the multi-bit sigma-delta control system has been designed, simulated, and prototyped. In the near future, the electronics and mechanical sensing element will be integrated and characterized as a roll-rate sensor. The resolution, scale factor linearity, and dynamic range will be determined and fed back into the design and simulation process. At the end of this development, a completely packaged and operational device will be made available for use in missile applications.

9. References

1. K. Funk, H. Emmerich, A. Schilp, M. Offenberg, R. Neul, and F. Lärmer, "A surface micromachined silicon gyroscope using a thick polysilicon layer," *Technical Digest IEEE International MEMS '99 Conference*, pp. 57-60, 1999.
2. W. A. Clark, R. T. Howe, and R. Horowitz, "Micromachined z-axis vibratory rate gyroscope," *Technical Digest of the Solid-State Sensor and Actuator Workshop*, pp. 283-287, 1996.
3. M. Kranz, and G.K. Fedder, "Micromechanical vibratory rate gyroscopes fabricated in conventional CMOS," *Symposium Gyro Technology 1997*, pp. 3.0-3.8, 1997.
4. W. Geiger, B. Folkmer, U. Sobe, H. Sandmaier, and W. Lang, "New designs of micromachined vibrating rate gyroscopes with decoupled oscillation modes," *Sensors and Actuators A*, **66**, pp. 615-620, 1998.
5. T. J. Brosnihan, J. M. Bustillo, A. P. Pisano, and R. T. Howe, "Embedded interconnect and electrical isolation for high-aspect-ratio, SOI inertial instruments," *International Conference on Solid-State Sensors and Actuators Digest of Technical Papers*, **1**, pp. 637-640, 1997.
6. Y. Mochida, M. Tamura, and K. Ohwada, "A micromachined vibrating rate gyroscope with independent beams for the drive and detection modes," *Technical Digest IEEE International MEMS '99 Conference*, pp. 618-623, 1999.
7. J. B. Marion, S. T. Thornton, *Classical Dynamics of Particles & Systems*, Harcourt Brace Jovanovich, Inc., 1988.
8. T. Smith, O. Nys, M. Chevroulet, Y. DeCoulon, and M. Degrauwe, "A 15b electromechanical sigma-delta converter for acceleration measurements," *Solid-State Circuits Conference Digest of Technical Papers*, pp. 160-161, 1994.
9. M. A. Lemkin, M. A. Ortiz, N. Wongkomet, B. E. Boser, and J. H. Smith, "A 3-axis surface micromachined $\Sigma\Delta$ accelerometer," *Solid-State Circuits Conference Digest of Technical Papers*, pp. 202-203, 457, 1997.